Proton-^{3}He scattering with antisymmetrized amplitudes at intermediate energy

M. J. Páez* and R. H. Landau
Department of Physics, Oregon State University, Corvallis, Oregon 97331
(Received 14 October 1983)

The elastic scattering of protons from ^{3}He is calculated with a microscopic, momentum space optical potential which incorporates the full spin dependence of the NN and p ^{3}He interactions. The theory includes antisymmetrized NN amplitudes, realistic neutron and proton distributions, nucleon recoil and binding energy shifts, Lorentz invariant angle transformations, t matrices with on-shell behavior from NN phase shifts, and off-shell behavior from a realistic separable potential model. Qualitative agreement is found with differential cross section and polarization data for $100 < T_p < 1000$ MeV.

I. INTRODUCTION

Although the idea of using proton reactions to probe the nucleus is not new, the different energy dependence of the spin, isospin, and exchange parts of the nucleon-nucleon interaction illuminates different facets of the reaction at intermediate energies than at low and high energies. In particular, recent experimental study of spin effects has led to extensive refinements of the NN effective interaction and the p-nucleus optical potential.[1]

Simultaneous with the above developments has been the fundamental progress made in understanding the pion-nucleus system[2]—particularly the momentum space optical potential. In this paper we join some of these π-^{3}He techniques[3] to those used in proton scattering.[4–6] This union is interesting since the nature of the two projectiles, and the techniques, are quite different.

By studying the p-^{3}He interaction we test multiple scattering theory and unravel a fascinating reaction mechanism in which nucleon, N*, and deuteron exchanges all contribute.[7–10] We also wish to advance the theory so that the hadron experiment may provide information on the ^{3}He nucleus. Specifically, large angle, intermediate energy proton scattering is sensitive to the nuclear wave function at momentum transfers considerably higher than the current electron measurements and without the annihilation problem inherent with pions. Although exchange currents also contribute to proton scattering, their effect is relatively smaller since the first order proton term is much larger. And since the spin of the ^{3}He nucleus resides on $\sim\frac{1}{3}$ of its nucleons (the two protons's spins are essentially paired to zero) there is the promise of utilizing the high spin dependence of the NN interaction to deduce the spin distribution.

The existing[11–21] and new[22] p-^{3}He cross section and polarization data are unusually complete in that they scan an energy range from $\sim$1–1000 MeV in both the forward and backward hemispheres. At low energies ($T_p \lesssim 10$ MeV), resonating group[23] and variational[24] calculations succeed in reproducing the data and find that large antisymmetrization effects can be modeled by an effective potential having opposite signs for even and odd orbital angular momenta.[25] By 20 MeV, good phenomenological fits are possible if the optical potential contains an exchange term.[6] As the energy gets higher, diffractive features appear and a distinct, backward peak is evident by 400 MeV. At 1 GeV the cross sections are diffractive and Glauber or multiple diffraction theories should provide the best descriptions.[26–29]

The medium energy backward peaks are somewhat of a

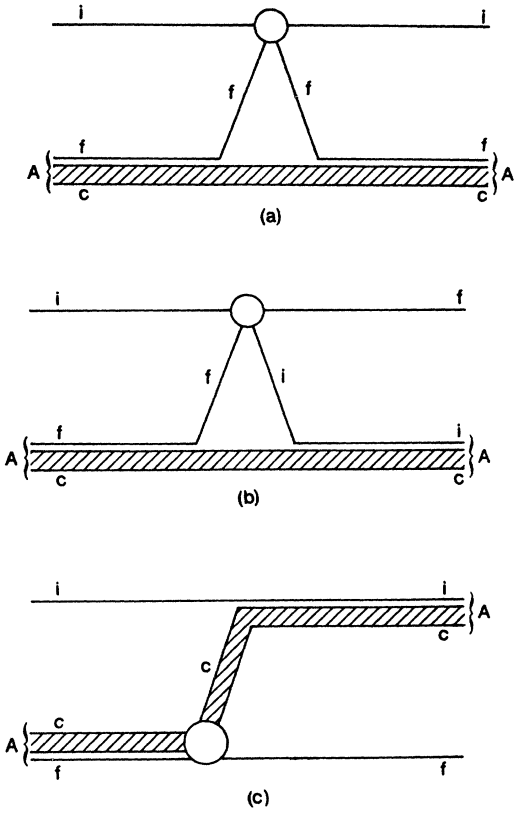

FIG. 1. Processes contributing to p-^{3}He elastic scattering (Ref. 8). (a) The "direct" scattering of projectile nucleon i with target nucleon f, the core c is passive; (b) The "exchange" part of the single scattering term in which the projectile and struck nucleons interchange; and (c) heavy particle "c" exchange or stripping, the final nucleon f has not been struck.

mystery. The momentum transferred is too large for the direct term [Fig. 1(a)] or any of its multiply-scattered iterations to be significant. Although the Pauli principle would indicate that NN exchange [Fig. 1(b)] is as likely as direct scattering,[30] this is difficult to include reliably in a practical multiple scattering calculation. Consequently, more exotic effects, such as heavy particle[8] and N* exchanges[9,10] [Fig. 1(c)] are postulated, and often shown to be significant. Definitive conclusions, however, must await a more reliable evaluation of Figs. 1(b) and (c) and a more systematic theory for the entire process.

At present many more studies of the simpler p-^{4}He system exist; some are microscopic optical potentials,[31] some are diffraction theory,[29,30] and some are phenomenological fits with both the Schrödinger[6] and Dirac[5] equations. Up to 1 GeV, spin and exchange effects remain important. At the higher energies, evidence exists[32] that intermediate isobar states are contributing.

In Sec. II we formulate a microscopic first order optical potential for p^{3}He scattering. The major complication is handling the full spin $\frac{1}{2}\times\frac{1}{2}$ dependence of NN and p^{3}He interactions, and the four possible nuclear form factors. Since this is our first paper on this theory, we give some specifics in Sec. II and some details in Appendices A and B. In Sec. III we examine the sensitivity of our theory to various assumptions and then compare the predicted $d\sigma/d\Omega$ and $P(\theta)$ to data for $100<T_{\rm p}<1000$ MeV. Section IV provides a summary and our conclusions.

II. FORMULATION

The most general form for the scattering amplitude of two spin $\frac{1}{2}$ particles consistent with rotational invariance, parity conservation, time-reversal invariance, and the generalized Pauli principle (isospin invariance) is

$$M=\tfrac{1}{2}[(A+B)+(A-B)\vec{\sigma}_1\cdot\hat{n}\,\vec{\sigma}_2\cdot\hat{n}+(C+D)\vec{\sigma}_1\cdot\hat{m}\,\vec{\sigma}_2\cdot\hat{m}+(C-D)\vec{\sigma}_1\cdot\hat{l}\,\vec{\sigma}_2\cdot\hat{l}+E(\vec{\sigma}_1+\vec{\sigma}_2)\cdot\hat{n}+F'(\vec{\sigma}_1-\vec{\sigma}_2)\cdot\hat{n}]\ , \tag{2.1}$$

where $\hat{n}$, $\hat{m}$, and $\hat{l}$ are the unit vectors,

$$\hat{n}=\frac{\vec{k}_i\times\vec{k}_f}{|\vec{k}_i\times\vec{k}_f|},\quad \hat{l}=\frac{\vec{k}_i+\vec{k}_f}{|\vec{k}_i+\vec{k}_f|},\quad \hat{m}\frac{\vec{k}_f-\vec{k}_i}{|\vec{k}_f-\vec{k}_i|}\ , \tag{2.2}$$

where $(\vec{k}_i,\vec{k}_f)$ is the (initial, final) center of mass (c.m.) momentum, and the amplitudes $A-F'$ are functions of $\vec{k}_f$ and $\vec{k}_i$ but not spin.[33] For identical particles (e.g., two nucleons) the F' term vanishes via the generalized Pauli principle.

A. Optical potential

We describe p-^{3}He scattering via an optical potential constructed from nucleon-nucleon amplitudes having the full structure (2.1) in the NN c.m. The lowest order optical potential is the expectation value of the proton-nucleon t matrix in the nuclear ground state. In the factorization approximation it has the form

$$\begin{aligned}U(\vec{k}'\,|\,\vec{k})\simeq U^1(\vec{k}'\,|\,\vec{k})=\langle\psi_A\,|\,t^{\rm pN}\,|\,\psi_A\rangle\approx N\{&t^{\rm pn}_{A+B}\,\rho^{\rm n}_{\rm mt}(q)+[t^{\rm pn}_{A-B}\vec{\sigma}_{\rm p}\cdot\hat{n}\,\vec{\sigma}_{\rm n}\cdot\hat{n}+t^{\rm pn}_{E}\vec{\sigma}_{\rm n}\cdot\hat{n}+t^{\rm pn}_{C+D}\vec{\sigma}_{\rm p}\cdot\hat{m}\,\vec{\sigma}_{\rm n}\cdot\hat{m}\\&+t^{\rm pn}_{C-D}\vec{\sigma}_{\rm p}\cdot\hat{l}\,\vec{\sigma}_{\rm n}\cdot\hat{l}+t^{\rm pn}_{CD}(\vec{\sigma}_{\rm p}\cdot\hat{m}\,\vec{\sigma}_{\rm n}\cdot\hat{l}+\vec{\sigma}_{\rm p}\cdot\hat{l}\,\vec{\sigma}_{\rm n}\cdot\hat{m})]\rho^{\rm n}_{\rm sp}(q)\\&+t^{\rm pn}_{E}\vec{\sigma}_{\rm p}\cdot\hat{n}\rho^{\rm n}_{\rm mt}(q)\}+\left\{\begin{matrix}N\to Z\\ {\rm n}\to{\rm p}\end{matrix}\right\}\ .\end{aligned} \tag{2.3}$$

The $t_{A-B}, t_{C-D}, \ldots$, terms are proportional to linear combinations of the A, B, C, D, E, and F terms of (2.1) and are given explicitly in Eqs. (2.10)–(2.13).

We remind the reader that $U^{(1)}$ is complex (absorptive) only because the elementary t matrices are complex. In turn, $t^{\rm NN}$ is complex whenever the energy is physical, i.e., total energy greater than twice the rest mass. Thus, the absorption in $U^{(1)}$ accounts for the presence of nucleon knockout or quasielastic scattering[3] with the elastic $t^{\rm NN}$. And indeed, with the three body choice of energy [Eq. (2.15)], $U^{(1)}$ becomes real if the projectile energy is lower than the nucleon separation energy E_B. Of course we also include pion production as an open channel by using NN phases which become complex at the elementary π production threshold. This is, however, a less direct contribution to the reactive part of our potential.

The off-energy-shell, proton-nucleon t matrices in (2.3) are functions of projectile and target nucleon momenta $\vec{k}$ and $\vec{p}_0$ momentum transfer $\vec{q}=\vec{k}'-\vec{k}$, and subenergy ω, e.g.,

$$t^{\rm pn}_{A+B}=\langle\vec{k}',\vec{p}_0-\vec{q}\,|\,t^{\rm pn}_{A+B}(\omega)\,|\,\vec{k},\vec{p}_0\rangle\ . \tag{2.4}$$

Here, $\vec{p}_0$ is a choice for the target nucleon momentum

$$\vec{p}_0=-\frac{\vec{k}}{A}+\frac{A-1}{2A}\vec{q}\ ,$$

which optimizes the factorization approximation used to derive (2.3).[2,3] In this approximation the nuclear structure enters only via $\rho_{\rm mt}(q)$ and $\rho_{\rm sp}(q)$, the form factors describing the distribution of nucleon matter and spin within the nucleus. Although the techniques we outline here are also valid if actual wave functions were used to describe the three nucleon system, the simpler equation (2.3) permits a direct utilization of the measured electromagnetic form factors.

It is possible to hypothesize the off-energy-shell behavior of a t matrix in any reference frame. We believe it best, however, to do so in the two-body c.m., where potential theory can serve as a physically motivated guide. For this reason, we relate the t matrices of Eqs. (2.3) and (2.4) (in the p-He c.m.) to off-shell t matrices (in the NN c.m.) via

$$\langle \vec{k}',\vec{p}' \,|\, t(\omega) \,|\, \vec{k},\vec{p} \rangle = \gamma_{\rm LPT} \langle \vec{\kappa}' \,|\, \tilde{t}(\tilde{\omega}) \,|\, \vec{\kappa} \rangle \ , \tag{2.5}$$

$$\gamma_{\rm LPT} = \left[\frac{E_p(\kappa)E_p(\kappa')E_N(\kappa)E_N(\kappa')}{E_p(k)E_p(k')E_N(p)E_N(p')} \right]^{1/2} , \tag{2.6}$$

where $\vec{\kappa}$ and $\vec{\kappa}'$ are the pN c.m. momenta appropriate to the pA momenta $(\vec{k},\vec{p}\,)$ and $(\vec{k}',\vec{p}\,')$, respectively, and $\gamma_{\rm LPT}$ arises from (on-shell) probability conservation.[34] The off-shell variation of the t matrices are now described by a separable potential in each eigenchannel $\alpha \equiv (J,L,S)$:

$$\langle \vec{\kappa}' \,|\, \tilde{t}[\tilde{\omega}(\kappa_0)] \,|\, \vec{\kappa} \rangle = \sum_\alpha \frac{g_\alpha(\kappa')g_\alpha(\kappa)}{g_\alpha^2(\kappa_0)} \times \langle \kappa_0 \,|\, \tilde{t}_\alpha[\tilde{\omega}(\kappa_0)] \,|\, \kappa_0 \rangle Y_L^M(\hat{\kappa}' \cdot \hat{\kappa}) \ , \tag{2.7}$$

where $\langle \kappa_0 \,|\, \tilde{t}_\alpha[\tilde{\omega}(\kappa_0)] \,|\, \kappa_0 \rangle$ is the on-shell amplitude. For this off-shell extrapolation we use the Graz potential[35] generalized up to K waves; the parameters are given in Table I. Although the NN potentials are fit to NN data for $T_p \lesssim 300$ MeV, they should provide a physical off shell variation for a much wider range.

The on-shell NN amplitudes, A–E in Eq. (2.1), are calculated from the Bystricky *et al.*[36] phase shift tabulation. The details are in Appendix A. Our basic two-body input contains full spin dependences, independent variations of the momenta, and energy variables as required by the Schrödinger theory, and is valid for $10 \le T_p \le 750$ MeV and all scattering angles. These features are incorporated directly into the momentum space potential.

We include the Pauli principle by using an antisymmetrized NN amplitude (e.g., t^{pp} is symmetric about 90°). This is equivalent to including direct scattering [Fig. 1(a)] and the exchange of the projectile and struck nucleon [Fig. 1(b)]. It does not, however, include antisymmetrization with unstruck nucleons (as in resonating group calculations), which can lead to heavy particle exchange (or stripping) [Fig. 1(c)]. Sherif *et al.*[6,8] have emphasized the importance of heavy exchanges for back angle scattering.

Our calculation does not include any second order corrections to the optical potential such as intermediate double charge exchange and NN correlations. Of this same order, and as emphasized by Gurvitz,[37] the optical potential which appears in the kernel in our Lippmann-Schwinger equation [Eq. (2.24)] should have the exchange part of the t^{NN} removed (a rather model-dependent procedure).

The NN c.m. momenta $\vec{\kappa}$ and κ' are determined via a covariant, on-mass-shell, "angle transformation":[2]

$$\vec{\kappa} = b(\theta)\vec{k} + c(\theta)\vec{k}' \ , \quad \vec{\kappa}' = b'(\theta)\vec{k}' + c'(\theta)\vec{k} \ , \tag{2.8}$$

where $b(\theta)$ and $c(\theta)$ are functions of the scattering angle in the pA system. The details are given in Appendix B.

Consequences of these transformations include the increase in the pN momenta κ and κ' (and pN subenergy $\tilde{\omega}$—see Fig. 2) as the p-^{3}He scattering angle increases and the mapping of backward p-^{3}He scattering ($\cos\theta = -1$) into backward pN scattering ($\cos\tilde{\theta} = -1$). In addition, when we form the three unit vectors $\hat{n}$, $\hat{m}$, and $\hat{l}$ in the NN c.m. (analogous to $\hat{n}$, $\hat{m}$, and $\hat{l}$ [Eq. (2.2)] in the pA c.m.), these will be linear combinations of $\hat{m}$ and $\hat{l}$:

$$\tilde{n} = \frac{\vec{\kappa} \times \vec{\kappa}'}{|\vec{\kappa} \times \vec{\kappa}'|} = \hat{n} \ , \tag{2.9a}$$

$$\tilde{m} = \frac{\vec{\kappa}' - \vec{\kappa}}{|\vec{\kappa}' - \vec{\kappa}|} = d(\theta)\hat{m} + e(\theta)\hat{l} \ , \tag{2.9b}$$

TABLE I. Graz potential parameters

$$g_L(\kappa) = [\beta_0^2 + \kappa^2]^{-1}, \quad L = 0 \ ;$$

$$g_L(\kappa) = \kappa^L(1+\gamma\kappa^2) \left[\prod_{n=0}^{L+1} (1+\beta_n\kappa^2) \right]^{-1} , \quad L \neq 0 \ .$$

All parameters in fm^2. F–K waves are the indicated generalization of the $^3D_2$ potential.

Eigenchannel	γ	β_0	β_1	β_2	β_3	β_4	β_5
$^3S_1$	0	1.43	0				
$^1S_0$	0	1.152	0				
$^1P_1$	1.0297	4.2965	0.0506	0.0493			
$^3P_0$	4.3036	4.0351	0.7292	4.3036			
$^3P_1$	0.9055	3.6475	0.0446	0.0412			
$^3P_2$	0.1514	0.4266	0.0634	0.0634			
$^1D_2$	0.4897	5.0341	0.1589	0.0705	0.0169		
$^3D_2$	0.7544	6.7807	0.1583	0.1583	0.0738		
all F	0.7544	6.7807	0.1583	0.1583	0.0783	0.5	
all G	0.7544	6.7807	0.1583	0.1583	0.0783	0.5	0.5

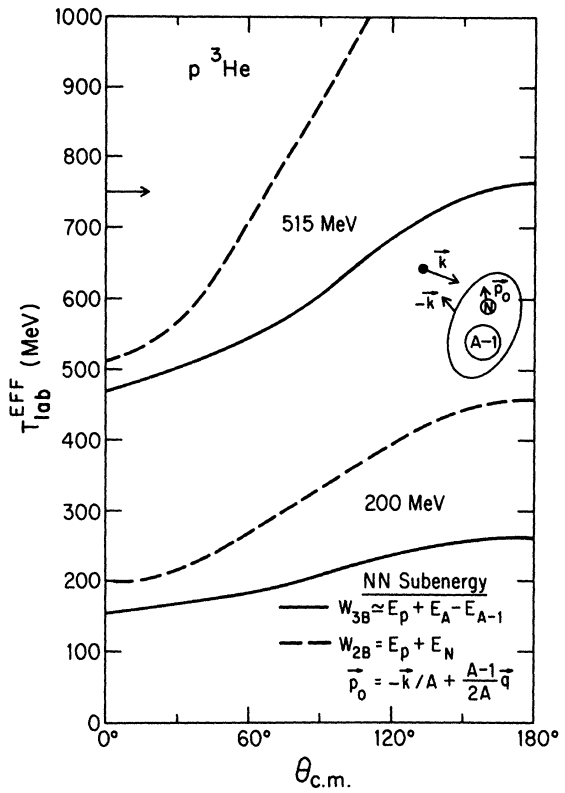

FIG. 2. The effective NN laboratory kinetic energy as a function of the p-^{3}He scattering angle for incident proton energies of 200 and 515 MeV. The solid curves result from the three-body choice of subenergy [Eq. (2.15)], and the dashed curves from the two-body energy [Eq. (2.14)]. The arrow indicates the highest energy for the BLL phase shift tabulation (Ref. 36).

$$\tilde{l}=\frac{\vec{\kappa}+\vec{\kappa}'}{|\vec{\kappa}+\vec{\kappa}'|}=f(\theta)\hat{l}+g(\theta)\hat{m}\ . \tag{2.9c}$$

[The functions $d(\theta)$–$g(\theta)$ are derived in Appendix B.] This mixing implies that $\langle\vec{\kappa}'|t|\vec{\kappa}\rangle$ has the form [Eq. (2.1)] in the NN c.m., only now with $\tilde{n}$, $\tilde{m}$, $\tilde{l}$, and, consequently, the $\vec{\sigma}\cdot\hat{m}\,\vec{\sigma}\cdot\hat{m}$ and $\vec{\sigma}\cdot\hat{l}\,\vec{\sigma}\cdot\hat{l}$ terms in the pA c.m. derived from mixed terms. The t matrix elements which appear in the optical potential [Eq. (2.3)] are given by

$$t^i_{C\pm D}=-(\gamma_{\rm LPT}/2\rho_E)\begin{cases} d^2(\theta_A)(C+D)+g^2(\theta_A)(C-D) & \text{(2.10a)}\\ f^2(\theta_A)(C-D)+e^2(\theta_A)(C+D)\,, & \text{(2.10b)}\end{cases}$$

$$t^i_E=-(\gamma_{\rm LPT}/2\rho_E)(bb'-cc')E\ , \tag{2.11}$$

$$t^i_{A\pm B}=-(\gamma_{\rm LPT}/2\rho_E)(A\pm B),\quad i=\text{pp,pn}\ , \tag{2.12}$$

$$t^i_{CD}=-(\gamma_{\rm LPT}/2\rho_E)[d(\theta)e(\theta)(C+D)+f(\theta)g(\theta)(C-D)]\ . \tag{2.13}$$

Here, $-(A,B,C,D,E)/2\rho_E$ are the amplitudes in the NN c.m. and we do not include any relativistic (Wigner) spin precession.

Of particular interest is the $t_{CD}\vec{\sigma}\cdot\hat{l}\,\vec{\sigma}\cdot\hat{m}$ terms of Eqs. (2.3) and (2.13) since it is of the form usually excluded by time reversal invariance. This seems peculiar since it arises from expressing the time-reversal-invariant $\vec{\sigma}\cdot\hat{l}\,\vec{\sigma}\cdot\hat{l}$ and $\vec{\sigma}\cdot\hat{m}\,\vec{\sigma}\cdot\hat{m}$ parts of the proton-nucleon amplitude in the proton-nucleus momenta variables. However, the full amplitude still obeys the time reversal condition,

$$T(\vec{k}',\vec{k},\vec{\sigma})=T(-\vec{k},-\vec{k}',-\vec{\sigma})\ ,$$

since t_{CD} reverses sign upon time reversal, $(d,e,f,g)\rightarrow(d,-e,f,-g)$. A further concern with this mixed term is that it leads to a very small mixing of the singlet and triplet states in p^{3}He scattering. It is small since $t_{CD}=0$ both for on-shell scattering and for the very important "diagonal" $|\vec{k}'|=|\vec{k}|$ scattering. Since this mixing complicates the reduction of the Schrödinger equation, we ignore its small effect on this initial study.

We need to still specify the NN subenergy $\tilde{\omega}$. We evaluate $\tilde{t}(\omega)$ with the two- and three-body choices[2,3] for $\tilde{\omega}$. ω_{2B} is the four-momentum of the initial projectile $k_{\rm p}$ and the active nucleon $P_{\rm N}$. ω_{3B} is the four-momenta of the projectile proton plus target nucleus (k_A) minus that of the passive core (P).

$$\omega^2_{2B}=s_0=(k^\mu_{\rm p}+p^\mu_{\rm N})^2$$
$$=2m^2_{\rm N}+2E_{\rm p}(k)E_{\rm N}(p_0)-2\vec{k}\cdot\vec{p}_0\ , \tag{2.14}$$

$$\omega^2_{3B}=(k^\mu_{\rm p}+k^\mu_A-P^\mu_{A-1})^2$$
$$=[E_{\rm p}(k_0)+E_A(k_0)-E_{A-1}(P)-|E_B|]^2-\vec{P}^2\ , \tag{2.15}$$

$$P^2=|-\vec{k}-\vec{p}_0-\vec{p}\,|^2$$
$$\simeq\left[\frac{A-1}{A}\right]^2[k^2+q^2/4+p^2_F+\vec{q}\cdot\vec{k}]\ . \tag{2.16}$$

ω_{3B} arising naturally in a three-body model of the optical potential[2] is important in ensuring elastic unitarity at lower energies, and is our preferred choice. p_F is a Fermi momentum which we choose as 185 MeV/c—appropriate for a nucleon in the nuclear surface, and E_B is an *effective* nucleon-core binding energy (we take it as "only" 5 MeV since nucleon-core interactions are known to partially cancel the naive three-body energy shift).

The difference between ω_{2B} and ω_{3B} is shown graphically in Fig. 2. ω_{3B} is always at least 40 MeV less and increases less rapidly with θ. Consequently, since our input $t^{\rm NN}$s are valid up to 750 MeV, and since we reach this limit for 550 MeV p-He scattering at 180°, our back angle results lose validity above that energy. Fortunately, multiple, smaller angle pN scattering is dominant at large pA angles, and there may be some validity to our results up to ~900 MeV.

B. Three nucleon form factors

We use the four form factors shown in Fig. 3 to describe the neutrons's and protons's matter and spin distributions.[38] If we follow the anlaysis used in our pion study[3] and ignore exchange currents, we can relate them to the experimentally accessible charge form factors of ^{3}He and ^{3}H and the magnetic form factor of ^{3}He:

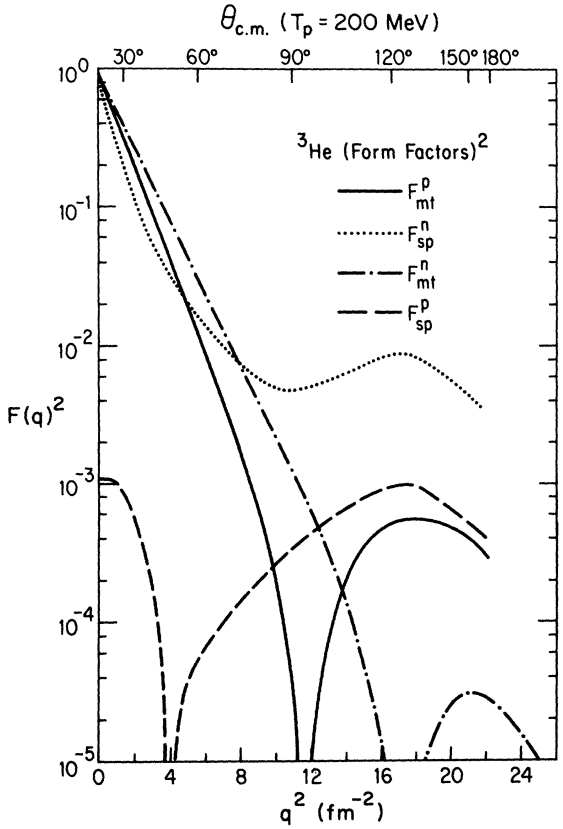

FIG. 3. The neutron and proton, matter and spin form factors for ^{3}He as deduced from EM form factors of ^{3}He and ^{3}H. The lower axis is momentum transferred squared, the upper, scattering angle for a 200 MeV beam. Note that F^n_{sp} appears unphysically large for high q^2 and is not used in the calculations.

$$\rho^{p,n}_{mt}(q)=F_{ch}(^3\mathrm{He},^3\mathrm{H})/f^p_c(q)\ , \tag{2.17}$$

$$\rho^n_{sp}(q)=2\xi\left[2F_{mag}(^3\mathrm{He})+\frac{4\mu_p}{3\mu_n}F_{ch}(^3\mathrm{He})-\frac{\mu_p}{3\mu_n}F_{ch}(^3\mathrm{H})\right]\ , \tag{2.18}$$

$$\rho^p_{sp}(q)=\xi[F_{mag}(^3\mathrm{He})-\tfrac{4}{3}F_{ch}(^3\mathrm{H})+\tfrac{1}{3}F_{ch}(^3\mathrm{H})]\ , \tag{2.19}$$

where μ_p and μ_n are the nucleons's magnetic moments,

$$\xi=\frac{\mu_n}{2(\mu_p+2\mu_n)f^p_c(q)}, \qquad \mu_p=2.793,\ \ \mu_n=-1.913\ , \tag{2.20}$$

and $f^p_c(q)$ is the elementary proton's form factor

$$f^p_c(q)=\left[1+\frac{q^2}{18.2\ \mathrm{fm}^{-2}}\right]^{-2}. \tag{2.21}$$

For "small" q^2 ($\lesssim 20$ fm^{-2}), the ^{3}He form factors are taken from McCarthy *et al.*,[39]

$$F_{ch,mag}(^3\mathrm{He})=\exp(-a^2q^2)-b^2q^2\exp(-c^2q^2)+d\exp\left[-\left[\frac{q-q_0}{p}\right]^2\right], \tag{2.22}$$

$$a_{c,m}=(0.675,0.654),$$
$$b_{c,m}=(0.366,0.456)\ \mathrm{fm}\ ,$$
$$c_{c,m}=(0.836,0.821)\ \mathrm{fm},$$
$$d_{c,m}=(-6.78\times10^{-3},0)\ ,$$
$$q_0=3.98\ \mathrm{fm}^{-1},\ \ p=0.90\ \mathrm{fm}^{-1}\ ,$$

and for large q^2 ($18\le q^2\le 80$ fm^{-2}) from Arnold *et al.*:[40]

$$F_{ch}(^3\mathrm{He})=[(1+\tau)/(1+\tau\mu^2_{He})]^{1/2}A^{1/2}$$
$$A^{1/2}=\alpha\exp(-\beta q^2),\qquad \alpha=0.034,\ \ \beta=0.1059\ \mathrm{fm}^2\ , \tag{2.23}$$
$$\tau=q^2/4m^2_{He},\ \ \mu=-2.1\ .$$

Unfortunately, some of the assumptions used to deduce these form factors become weak at very large momenta transfers[38] and further choices are needed. ρ^p_{mt} (solid curves in Fig. 3) is thus quite realistic and reliable. If we take the ^{3}H charge form factor of Collard *et al.*,[41] and extrapolate it for $q^2>15$ fm^{-2} with the three nucleon wave functions of McMillan,[42] we obtain ρ^n_{mt} (dot-dashed curve) which is less reliable beyond 15 fm^{-2}. If we substitute these two charge and one magnetic form factors into Eqs. (2.17)—(2.21) we obtain ρ^n_{sp} (dotted curve) and ρ^p_{sp} (dashed curve). We see that ρ^n_{sp} appears unphysically large in the extrapolated $q^2>12$ fm^{-2} region probed by large angle proton scattering and consequently we set $\rho^n_{sp}=\rho^n_{mt}$. Likewise, since the deduced proton spin form factor only becomes significant for $q^2>12$ fm^{-2}, i.e., where the empirical input used to derive it becomes unreliable, we decrease noise by setting $\rho^p_{sp}\equiv 0$.

To proceed we must make these choices regarding the nuclear form factors. After our basic calculation is understood and perfected, we will deduce these form factors from the proton scattering data or 3N wave functions, and remove meson exchange current effects.

C. The Lippmann-Schwinger equation

We wish to solve the Lippmann-Schwinger equation with relativistic kinematics,[34]

$$R(\vec{k}'\,|\,\vec{k})=U(\vec{k}'\,|\,k)+P\int\frac{d^3pU(\vec{k}'\,|\,\vec{p}\,)R(\vec{p}\,|\,\vec{k}\,)}{E(k_0)-E(p)}\ , \tag{2.24}$$

$$E(k_0)=E_p(k_0)+E_A(k_0)=(m^2_p+k^2_0)^{1/2}+(m^2_A+k^2_0)^{1/2}\ , \tag{2.25}$$

for a potential with the general spin dependence of Eq. (2.3). Although this seems not to have been previously accomplished, the framework can be found in the very useful NN study of Haftel and Tabakin.[43] They indicate the appropriate partial wave expansions of the potentials or amplitudes in terms of spin-angle functions:

$$M(\vec{k}',\vec{k}) \equiv \begin{Bmatrix} U(\vec{k}' \mid \vec{k}) \\ R(\vec{k}' \mid \vec{k}) \end{Bmatrix} = \frac{2}{\pi} \sum_{\alpha,L,L',M} M^{\alpha}_{LL'}(k' \mid k) \mathscr{Y}^{JM}_{LS}(\hat{k}') \mathscr{Y}^{\dagger JM}_{L'S}(\hat{k}) \ . \tag{2.26}$$

After substitution into (2.24), for each J value there results five partially coupled, integral equations:

$$R^{\alpha}_{LL'}(k' \mid k) = U^{\alpha}_{LL'}(k' \mid k) + \frac{2}{\pi} \sum_{l} P \int_0^{\infty} \frac{dp\, p^2 U^{\alpha}_{Ll}(k' \mid p) R^{\alpha}_{lL'}(p \mid k)}{E(k_0) - E(p)} \ . \tag{2.27}$$

For $S=1$, $L=J+1$ and $J-1$ are coupled by the tensor forces as indicated in Tables II and III. The numerical techniques used to solve these equations are similar to those in Ref. 43 and the computer code LPOTT.[44]

Since the proton and ^{3}He nucleus are not identical, there is no generalized Pauli principle to eliminate the coupling between p ^{3}He singlet and triplet states. However, since we use a first order optical potential proportional to the elementary NN t matrix [Eq. (2.3)] there is still no singlet-triplet coupling.

The on-shell values of $\hat{R}$ matrix are related to the pA phase shifts (Blatt-Biedenharn convention) via

$$\tan\delta^{\alpha}_{L=J\pm1} = -\rho_{\rm LPT} \left[R^{\alpha}_{J-1,J-1}(k_0 \mid k_0) + R^{\alpha}_{J+1,J+1} \mp \frac{R^{\alpha}_{J-1,J-1} - R^{\alpha}_{J+1,J+1}}{\cos 2\epsilon_{\alpha}} \right] \Big/ 2 \ , \tag{2.28}$$

$$\tan 2\epsilon_{\alpha} = \frac{2R^{\alpha}_{J-1,J+1}(k_0 \mid k_0)}{R^{\alpha}_{J-1,J-1} - R^{\alpha}_{J+1,J+1}} \ , \tag{2.29}$$

$$\rho_{\rm LPT} = 2k_0\mu(k_0) \ , \tag{2.30}$$

$$\mu(k_0) = E_{\rm p}(k_0)E_A(k_0)/[E_{\rm p}(k_0) + E_A(k_0)] \ . \tag{2.31}$$

D. Partial wave matrix elements

To solve the Lippmann-Schwinger equations [(2.27)] we need to evaluate the partial wave elements of V and R for a completely general spin dependent potential. While it is possible to evaluate directly the elements, e.g.,

$$U^{\alpha}_{LL'}(k' \mid k) = \frac{\pi}{2} i^{L'-L} \int d\hat{k}\, d\hat{k}'\, \mathscr{Y}^{\dagger JM}_{LS}(\hat{k}') U(\vec{k}' \mid \vec{k}) \mathscr{Y}^{JM}_{L'S}(\hat{k}) \ , \tag{2.32}$$

an advance in our approach (which reduces complications and errors) is the realization that the p ^{3}He $R_{\nu'\nu}$ and $U_{\nu'\nu}$ must have the same expansions as the NN amplitude[45] [Eqs. (A8)–(A14)]. Schematically, this is

$$U_{\nu'\nu}(\vec{k}' \mid \vec{k}) = \sum_{LL'J} B^{\nu'\nu}_{LL'} U^{\alpha}_{LL'}(k' \mid k) P^M_L(\cos\theta) \ , \tag{2.33}$$

which permits direct projections for $U^{\alpha}_{LL'}(k' \mid k)$.

In Fig. 4 we plot $\mathrm{Re}U_{\nu'\nu}(\vec{k}' \mid \vec{k})$ for $k=k'=465$ MeV/c ($T_{\rm p}=200$ MeV) as a function of scattering angle $\theta_{kk'}$. The zeros seen in $U^{(1)}$ reflect those in $t^{\rm NN}$ and $\rho^{\alpha}(q)$.

TABLE II. Spin $\frac{1}{2}\times\frac{1}{2}$ amplitude codes.

$N_{\rm spin}$	S	$M^J_{L,L'}$	Stapp
1	0	$M^L_L \equiv M^L_{LL}$	αL
2	1	M^L_{LL}	αLL
3	1	M^{L+1}_{LL}	$\alpha_{L,L+1}$
4*	1	$M^{L+1}_{L+2,L}$	$\alpha^{L'-1}(L'=L+2)$
5	1	$M^{L+1}_{L+2,L+2}$	$\alpha_{L',L'-1}(L'=L+2)$
6	1	$M^{L+1}_{L,L+2}$	α^{L+1}

*$M^{L+1}_{L+2,L} = M^{L+1\,\dagger}_{L,L+2}$ $\quad M^0_{00} = M^{-1}_{00} = M^{-1}_{0\pm2} = M^0_{1-1} = M^0_{02} = 0$

For example, at 90° the form factors vanish (for illustration we set $\rho^{\rm n}_{\rm mt} = \rho^{\rm n}_{\rm sp} = \rho^{\rm p}_{\rm mt}$), and near 60° and 120° different parts of $t^{\rm NN}$ vanish. The dots indicate the precision of our numerical projections at reproducing these data. The only noticeable inaccuracies occur at large angle zeros in $U_{\nu'\nu}$ which ultimately get filled by the nonzero potential contributions and multiple scattering.

III. RESULTS

We solved for all possible spin observables for $10 \lesssim T_{\rm p} \lesssim 1000$ MeV. In Sec. III A we examine the effects of different theoretical assumptions, keeping the energy fixed at 200 MeV. In Sec. III B we present a comparison of predictions for $d\sigma/d\Omega$ and $P(\theta)$ at nine energies for which data are available.

A. Sensitivity

One of the fundamental questions for this initial study is how the spin structure of $U(\vec{k}' \mid \vec{k})$ and $t^{\rm NN}$ influence p ^{3}He scattering. In Fig. 5 we answer this for $d\sigma/d\Omega$ and in Fig. 6 for the polarization $P(\theta)$. On the left-hand sides of these figures we alternately employed (i) spin $0\otimes0$; or (ii) spin $0\otimes\frac{1}{2}$; or (iii) spin $\frac{1}{2}\otimes\frac{1}{2}$ forms of the Lippmann-

TABLE III. NN coupled channels, $2S+1_{L_J}$, $M_{\rm pp} = M^{I=1}$, $M_{\rm pn} = \frac{1}{2}(M^{I=1} + M^{I=0})$.

$I=0$		$I=1$
$^3S_1 + {}^3D_1$ $M^1_{00} + M^1_{22}$	$^3I_7 + {}^3K_7$	$^3P_2 + {}^3F_2$
		$^3F_4 + {}^3H_4$
$^3D_3 + {}^3G_3$ $M^3_{22} + M^3_{44}$	$^3G_5 + {}^3I_5$	$^3H_6 + {}^3J_6$

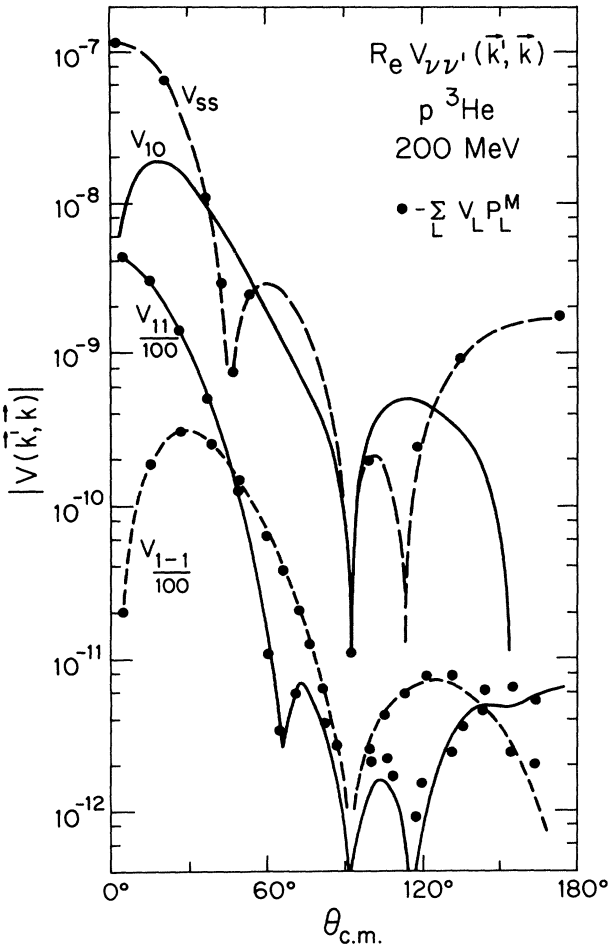

FIG. 4. Some p ^{3}He momentum space optical potential elements in the spin basis for $|\vec{k}'| = |\vec{k}| = k_0$. The dots indicate the precision of the numerical partial wave projections in reproducing these potentials. The universal zero at $\sim 90°$ occurs since all nuclear form factors are set equal here and vanish at this q.

Schwinger equations, i.e., potentials with (i) only the central term, t_{A+B} in Eq. (2.3); or (ii) with central plus spin orbit ($t_E \vec{\sigma}\cdot\hat{n}$); or (iii) full spin dependence. As witnessed by the difference of the 0×0 curve from the others (and from the data), spin effects are large [$P(\theta)\equiv 0$ for 0×0]. If we describe the scattering as $0\times\frac{1}{2}$, the spin dependence only arises from the spin-orbit, E, term of the NN amplitude. Yet since both the beam and target have spin we must choose how to turn off one of them. If we set σ_2, the target spin equal to zero [keep only the $t_E \vec{\sigma}_p\cdot\hat{n}\rho^n_{mt}$ in (2.3)], we obtain the dashed curves. This clearly does not produce enough scattering—but does predict a $P(\theta)$ of the same shape as the full calculation. If, as an exercise, we set target and projectile spins equal, $\sigma_1=\sigma_2$, then both the matter and spin distributions of the nucleus contribute to the spin-orbit term, and we obtain the dot-dashed curves in Figs. 5 and 6. The $d\sigma/d\Omega$ so produced is surprisingly similar to the full calculation, yet the $P(\theta)$ is rather poor at larger angles. Evidently the spin-orbit potentials are crucial, with the tensor potentials also playing a significant role—particularly at large angles.

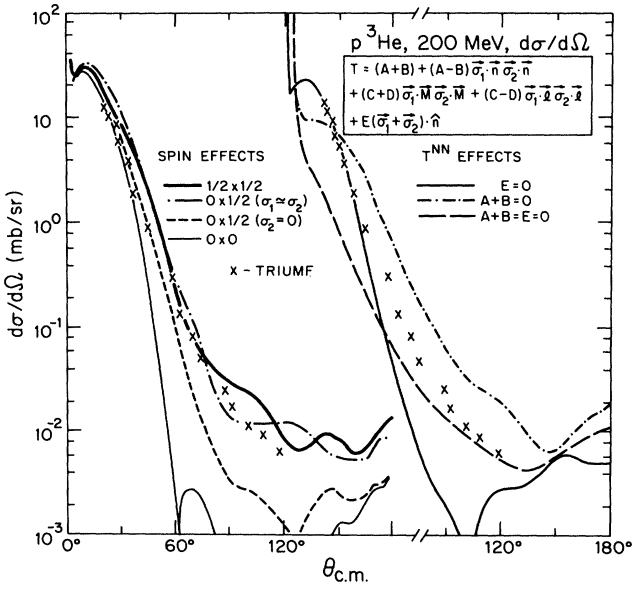

FIG. 5. Spin dependence of the predicted p-^{3}He differential cross sections at 200 MeV. The curves on the left result from progressively decreasing the number of spin variables in the Schrödinger equation ($\sigma_1\simeq\sigma_2$ treats projectile and nuclear spins as identical and is obviously unrealistic). The curves on the right-hand side result from selectively suppressing various terms in the elementary NN t matrix [Eq. (2.1)]. The data are from Hasell *et al.* (Ref. 22).

On the right-hand sides of Figs. 5 and 6 we show the effect of selectivity including different parts of the elementary nucleon-nucleon amplitude (2.1) while still performing the full $\frac{1}{2}\times\frac{1}{2}$ calculation. Again the E term in t^{NN} is large in the midangle $d\sigma/d\Omega$ and crucial in $P(\theta)$. The pure tensor terms produce strong mid-to-large angle scattering (dashed curves). In fact, $d\sigma/d\Omega$ with just tensor plus spin orbit is larger than with the full calculation whereas $P(\theta)$ is somewhat smaller.

The large strength of each spin term indicates that the rather smooth cross sections are actually the sum of five highly oscillatory terms (much like the potentials of Fig.

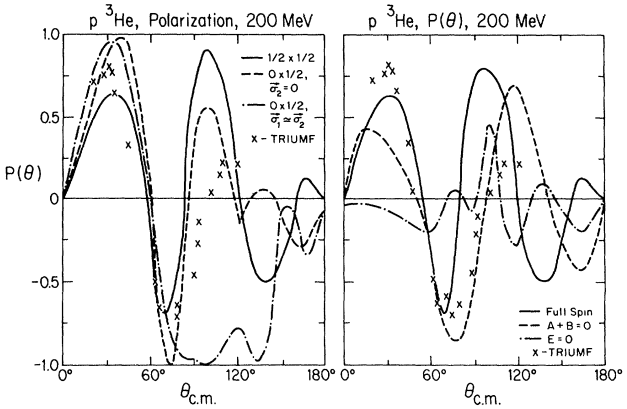

FIG. 6. The same as in Fig. 5 except now for the polarization $P(\theta)$.

4), with the deep minimum in any one filled by the others. By upsetting this somewhat delicate balance quite different results are obtained.

While some of the midangle structure is caused by spin scattering, we see in Fig. 7 that some is caused by multiple scattering (MS). The single scattering (SS) contribution, i.e., the Born term of (2.27), contains the zero of the ^{3}He form factors (we have set $\rho^n_{mt}=\rho^n_{sp}=\rho^p_{mt}$, and $\rho^p_{sp}=0$ here). The zero is filled predominantly by double scattering (DS), with the remaining MS sill significant even at small angles—a structure quite different from the Glauber theory. The dotted curve in Fig. 7 shows the effect of using the Kerman-McManus-Thaler[34] (KMT) rescaling, which reduces all multiple scatterings by $(A-1)/A=\frac{2}{3}$. This effect will not change any conclusions.

It is also possible to notice in Fig. 7 that the relatively large back angle cross section—which at higher energies turns into an actual peak—is present even in the single scattering term. This reflects their origin in the antisymmetrization of the elementary NN amplitude.

It is all too evident in the preceding figures that agreement with these 200 MeV TRIUMF data[22] is not very good at small angles (unless we turn off the spin—in which case the large angle cross sections are too small). While this is not surprising for our first attempt with an unadjusted theory, we need to examine the variations in our results at other energies and to theoretical assumptions before drawing conclusions. For example, we see in Fig. 8 that the choice of the three-body (preferred) or two-body energy [Eqs. (2.14) and (2.15)] produces a relatively minor variation, whereas the angle and momenta transformation [Eq. (2.8)] does produce a major increase in back angle scattering, as compared to the naive approach (solid curve).

In the upper part of Fig. 9 we see the effect on $d\sigma/d\Omega$ of assuming different forms for those ^{3}He form factors not well determined at these large q values. A similar study is given in Fig. 10 for the polarization. The solid curves in the upper part of Fig. 9 refer to our preferred choice, $\rho^n_{sp}=\rho^n_{mt}\neq\rho^p_{mt}$. The dashed curve in Fig. 9 and the dot-dashed curve in Fig. 10 are obtained when independent forms [Eqs. (2.17)–(2.19)] are used for these three form factors. As expected in this latter case, where the large q behavior of ρ^n_{sp} is not realistic, peculiar behavior in $d\sigma/d\Omega$ and $P(\theta)$ is predicted [the $P(\theta)$ behavior is even qualitatively incorrect]. We see how proton scattering can extend our knowledge of the $3N$ form factors. We also note in the upper part of Fig. 9 (dot-dashed curve) that unphysically small cross sections would be predicted if we did not divide out the elementary proton form factor from the ^{3}He form factors.

In the lower part of Fig. 9 we note that an increase in the nuclear size ["a" parameter in (2.22)] can bring the forward 200 MeV peak into agreement with the TRIUMF

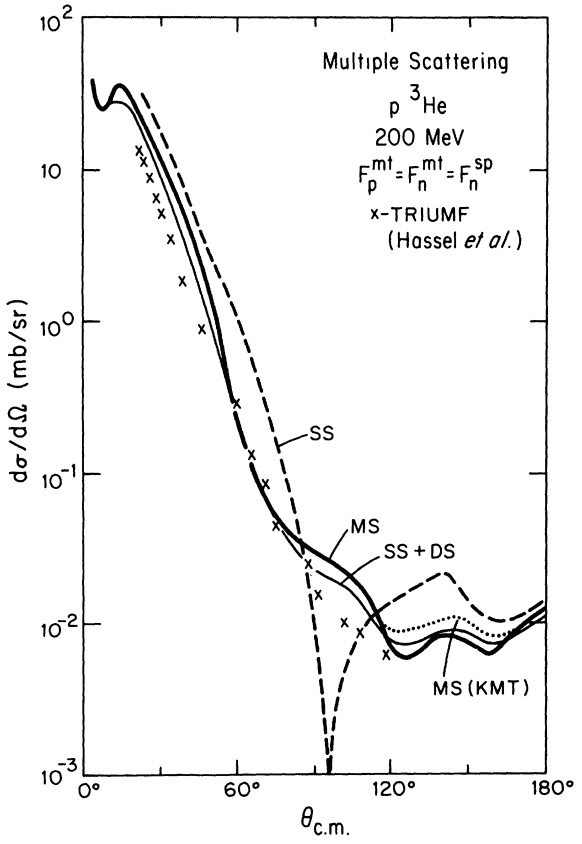

FIG. 7. The contribution of single scattering (SS), double scattering (DS), and multiple scattering (MS). The dotted curve is MS with the KMT $(A-1)/A$ reduction of multiple scattering.

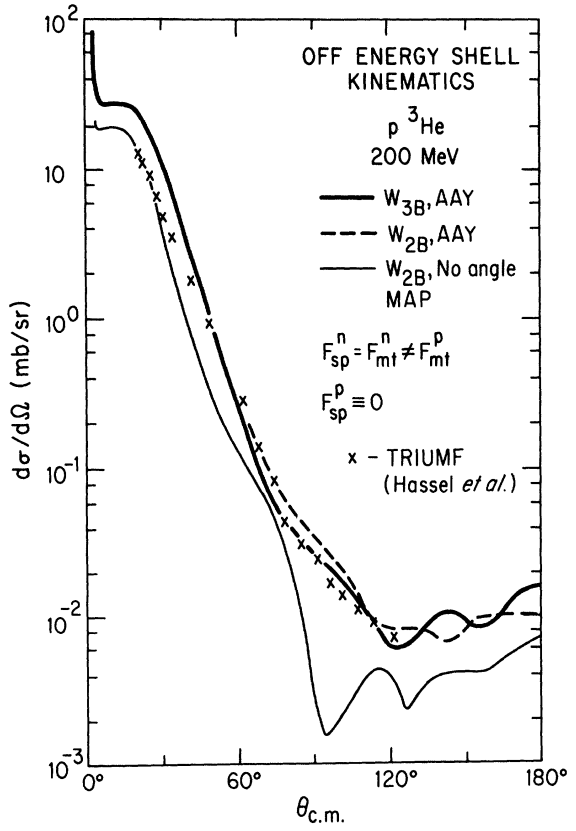

FIG. 8. The importance of the choice of two-body subenergy, ω_{2B},ω_{3B}, and of angle transformation for 200 MeV scattering. The light solid curve is the naive choice, ω_{2B} and $\theta_{NN}=\theta_{pHe}$ (no angle transformation).

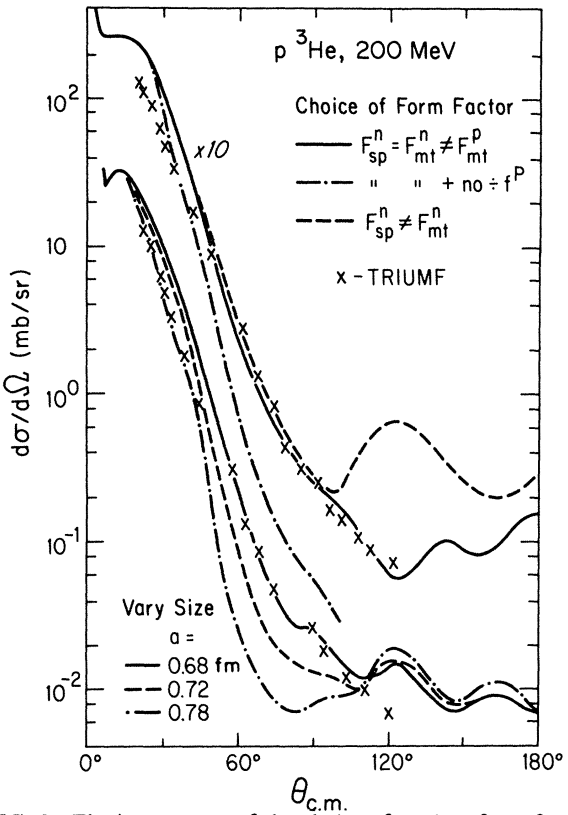

FIG. 9. The importance of the choice of nuclear form factors (upper curves) and of nuclear size variation on p-^{3}He scattering at 200 MeV. The upper solid curve is the preferred, $F^n_{sp}=F^n_{mt}\neq F^p_{mt}$, $F^p_{sp}=0$; the upper dot-dashed curve results if the elementary nucleon form factor is not removed from the ^{3}He form factors; and the upper dashed curve results if the spin form factors postulated in Eqs. (2.18) and (2.19) are employed (these are unrealistic at large q^2). The size parameter varied in the lower curves is that in Eq. (2.22).

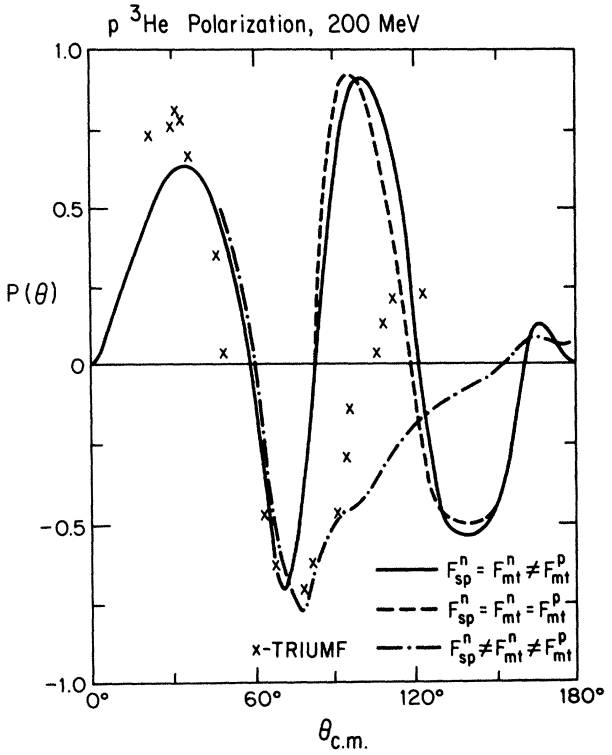

FIG. 10. The same as in the upper part of the Fig. 9, except now for $P(\theta)$.

data—but only at the expense of the midangle region. Yet since agreement is found at other energies, further study (e.g., other t matrices) is needed.

B. Energy survey

In Figs. 11 and 12 we show theoretical and experimental $d\sigma/d\Omega$ for energies varying from 100 to 1000 MeV. The large energy and angular regions covered by these data[11–20] are clearly impressive, as are their quality. The new TRIUMF data[22] fill in the intermediate energy regime. The solid curves are our full calculation with different form factors for the neutron and proton distributions, the dashed curves have the three nuclear form factors equal. The differences in these curves set the scale for nuclear structure sensitivity as a function of energy. The dotted curves are the (antisymmetrized) single scattering contribution and indicate the relative importance of multiple scattering.

In general, the quality of agreement is not as good as found in p-heavy nucleus scattering at $T_p\gtrsim 500$ MeV.[4] Apparently, the physics for very light nuclei is quite different and the impulse approximation for $U^{(1)}$ does not work well until $T_p\simeq 300$ MeV [i.e., the region where the Bystricky, Lechanoine, and Lehar (BLL) phases[36] cause $\mathrm{Re}t^{pn}$ to change sign]. Yet the reader should also note that a tremendous energy and complete angular range is

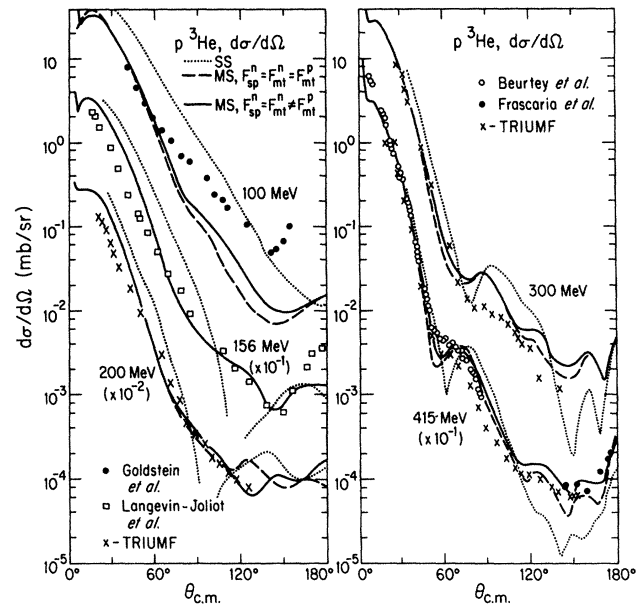

FIG. 11. The predicted p-^{3}He differential cross sections for $100\leq T_p\leq 415$ MeV. The solid curves are the preferred choice $F^n_{mt}\neq F^p_{mt}$, the dashed curves result for $F^n_{sp}=F^n_{mt}=F^p_{mt}$. The dotted curves correspond to single scattering, $T(\mathrm{p\,He})\simeq\sum t_i F_i(q)$.

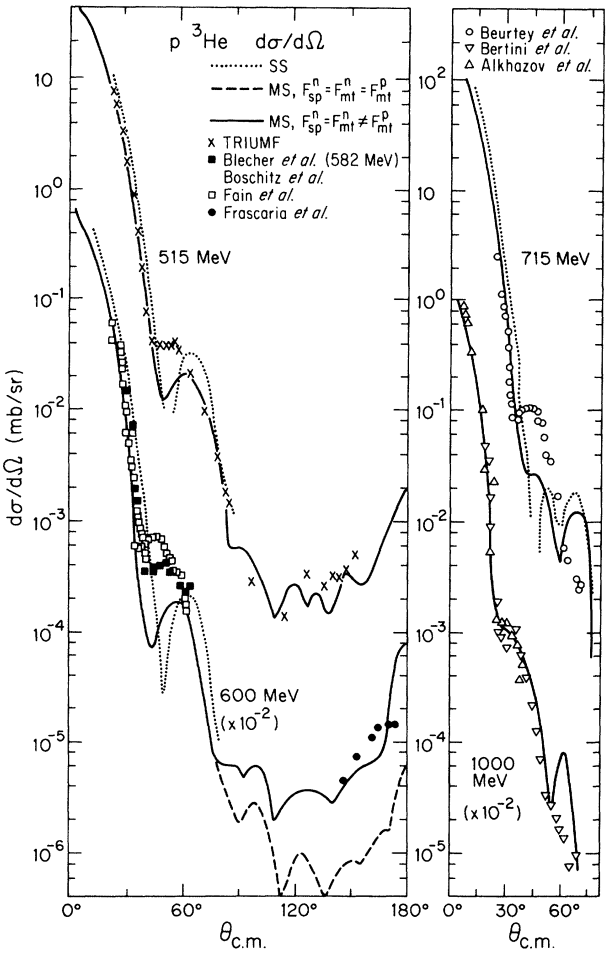

FIG. 12. The same as in Fig. 11, except now for $515 \leq T_p \leq 1000$ MeV.

being presented and that no adjustments are made—even in the four nuclear form factors which contain considerable uncertainty.

Intriguing features in Figs. 11 and 12 are the back angle peaks present in both the data and predictions. Although a first order optical potential must be suspect at such large momentum transfers, these peaks are somewhat of a reflection of our forward peaks in that they arise from the projectile struck-nucleon antisymmetry contained in t^{NN} (which explains their presence in SS too). Indeed, at 600 MeV we predict a back angle "diffraction" peak reminiscent of the backwards peaks in p-^{4}He scattering.

Back angle proton peaks have been identified with antisymmetry effects for at least thirty years. In a modern setting, Gurvitz *et al.*[30] postulated their origin in a back-peaked t^{NN}, and Alexander and Landau[31] calculated a similar peaking for p ^{4}He. However, several authors have also suggested their origin in N* and/or heavy particle exchange [Fig. 1(c)] in which the final proton is a spectator. Indeed, the recent distorted-wave Born approximation calculation of Sherif *et al.*[8] has shown that heavy particle exchange (stripping) is significant near 150 MeV. Since this exchange requires correlations, it is a necessary supplement to our $U^{(1)}$ calculation.

Another feature of interest in Figs. 11 and 12 is the gradual buildup of "diffractive" features with increasing energy. Yet since the minima arise from zeros in the ^{3}He form factors and the NN amplitudes, they cannot be identified with the interference of successive orders of multiple scattering—as Fig. 7 also makes clear.

For $T_p \lesssim 100$ MeV the microscopic $U^{(1)}$ is inadequate. This agrees with the good description of low energy p ^{3}He scattering by resonating group methods[23] which are sensitive to high order correlations (e.g., compound nucleus formation and heavy exchange). Indeed, since at low energies the p ^{3}He singlet and triplet states mix,[21] and since this mixing must arise from a term in the scattering amplitude (and thus optical potential) which behaves like $F(\vec{\sigma}_1-\vec{\sigma}_2)\cdot\hat{n}$, and since a term of this sort cannot occur in the first order potential [(2.3)], this proves that higher order corrections are important at low energies.

In the middle angle region, fair agreement is obtained from 156 to 415 MeV. From 500 to 700 MeV, the positions of the diffractive structures are predicted well, but not their magnitude. At 1000 MeV (which is beyond the limit of validity of our two-body input) a strikingly good fit is obtained out to $\sim 60°$. It appears that better agreement here may be obtained by using more correct nuclear form factors (e.g., some proton spin flip contribution may well raise the minima at 500—700 MeV), or possibly with intermediate isobar contributions.[32] Indeed, we can see a much greater sensitivity to our modest variation in form factors (solid versus dashed curves) at 600 MeV than at 200 MeV.

In Figs. 10 and 13 the predicted polarizations as a function of energy are shown. For $\theta \lesssim 60°$, the shape of $P(\theta)$

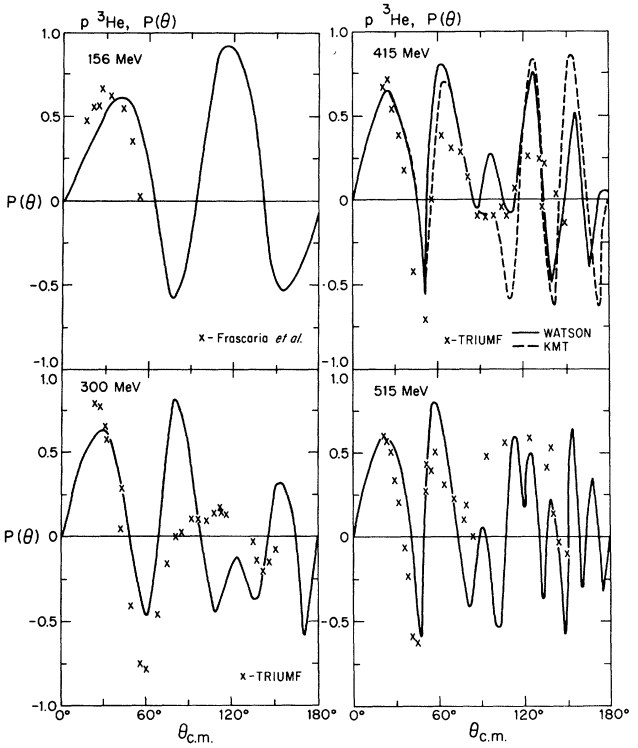

FIG. 13. Predicted p-^{3}He polarizations for $156 \leq T_p \leq 515$ MeV with $F^n_{mt} \neq F^p_{mt}$.

varies smoothly with energy (it is essentially just a function of t here) and the agreement between theory and experiment[15,22] is at least qualitative. At larger angles the predicted $P(\theta)$ becomes a highly oscillatory function, is much more sensitive to changes in the theory (e.g., tensor forces), and does not agree in any detail with experiment. Yet we can notice that there is much interference [$P(\theta)$ is the small difference of two large numbers] and that the experimental $P(\theta)$ varies least when the theory shows cancellations (e.g., 90° at 415 MeV).

Finally, in Fig. 14 are given the predicted total cross section for unpolarized target and beam (upper solid curve). The dashed curve shows the nonfolded, single scattering, impulse approximation result

$$\sigma(\text{p-}^3\text{He}) \simeq 2\sigma^{pp} + \sigma^{pn} .$$

Clearly, there is significant shadowing at the higher energies. The lower curve shows the predicted spin dependence of the total cross section.

IV. SUMMARY AND CONCLUSIONS

We have developed and applied a microscopic, first order optical potential for p-^{3}He scattering. The theory includes the full spin $\frac{1}{2}\times\frac{1}{2}$ dependence of the antisymmetrized NN amplitude,[36,33] off-energy-shell behavior based on a realistic, nonlocal, separable potential model,[35] realistic form factors for the distributions of neutron and proton matter and spin within the ^{3}He nucleus, and a three-body model for the optical potential which naturally incorporates important unitarity constraints[2] and nucleon binding and recoil. After developing new procedures, we are able to solve coupled Lippmann-Schwinger integral equations with relativistic kinematics in momentum space and thus include all orders of multiple scattering in which the nucleus remains in its ground state (presumably the dominant terms for coherent elastic scattering). This formulation thus includes all the theoretical nonlocalities, and energy, angle, spin, and momenta dependences ("angle transformations and energy shifts") in such a way that predictions are possible for all the p-^{3}He spin variables over the entire angular range and for energies between 100 and 1000 MeV.

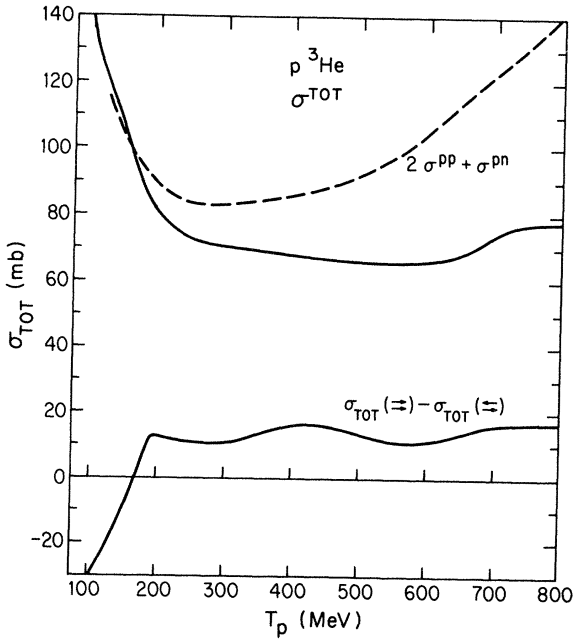

FIG. 14. p-^{3}He total cross sections for no polarizations (upper curves) and with polarization (lower curve). The dashed curve is the single scattering, impulse approximation result $2\sigma^{pp}+\sigma^{pn}$.

In comparing our predictions with the challenging number of complete and accurate data,[11–22] we find that our use of tensor forces and antisymmetrized nucleon-nucleon amplitudes provide partial explanation of the occurrence, the energy dependence, shape, and magnitude of the back angle p-^{3}He peaks. Yet since this simple application of the Pauli principle only amounts to the exchange of the projectile and struck nucleon, there are other exchanges which should be included. For example, heavy particle exchange is known to be significant in p-^{4}He backward scattering,[6,8] whereas N* exchange and constituents have also been postulated.[9,10] Furthermore, a higher order understanding of nucleon exchange requires the decomposition of t^{NN} into direct and exchange pieces[37]—a difficult task to accomplish in a model independent way at intermediate energies.[46]

Our analysis of the data also shows that the differential cross sections and polarizations display quite different physics. For example, the backward hemisphere's $P(\theta)$ is sensitive to tensor forces. The forward slopes of $d\sigma/d\Omega$ are not reproduced well until $T_p > 200$ MeV, possibly signaling the onset of validity of the impulse approximation or some shortcoming in the low energy nucleon-nucleon phase shifts[36] (different ones are currently under investigation).

Essentially, all predictions show a high sensitivity to the elementary neutron and proton matter and spin distributions. Yet since intermediate energy proton scattering explores these functions at very high momentum transfers, $q^2 \gtrsim 100$ fm^{-2}, only the proton matter (or ^{3}He charge[40]) form factors can be considered known. This naturally leads to several interesting possibilities. One is to "use" proton scattering to measure form factors—which of course assumes the theory is up to the task. Another is to employ theoretical three nucleon wave functions to generate the needed nuclear structure information. In any case, serious comparisons need to account for meson exchange currents in both the electromagnetic and strong form factors.

Although our calculation is just a first, elementary step, we believe the generality of this approach is quite promising and with improvements will be valuable for much of intermediate energy nucleon scattering. Indeed, other workers are independently applying similar formalisms to scattering from heavier nuclei.[47] To maintain this progress, some of our present work includes examinations of the ^{4}He(p,p) and ^{3}H(p,n)^{3}He reactions, the use of other, nucleon-nucleon phases, use of other off-shell models, and the incorporation of heavy particle exchanges.

ACKNOWLEDGMENTS

It is a pleasure to acknowledge helpful conversations with Dr. D. Hasell, Dr. A. Stetz, Dr. W. T. H. van Oers, Dr. J. Tostevin, Dr. J. Greben, Dr. P. Tandy, and Dr. R. C. Johnson. Special gratitude is due to Dr. Hasell and Dr. van Oers for providing and stimulating us with their data before publication. We also wish to thank the University of Surrey and TRIUMF for their hospitality and support during visits. Major fundings were supplied by the National Science Foundation, the Universidad de Antioquia, and the Oregon State University Research Office.

APPENDIX A: SPIN $\frac{1}{2}\times\frac{1}{2}$ AMPLITUDES FROM PHASE SHIFTS

We follow the formalism of Stapp *et al.*,[48] extended by Bystricky, Lehar, and Winternitz,[33] for the NN amplitudes, $A-E$ of Eq. (2.1). In the singlet ($S=0$) state, $J=L$ and there is only one amplitude. In the triplet ($S=1$) state, $J=L\pm1,L$ and we need five amplitudes. In Table II we enumerate amplitudes, relating Stapp's amplitudes α_{ij}, Haftel and Tabakin's (Ref. 43) $M^J_{L,L'}$, and LPOTT's (Ref. 44) $N_{\rm spin}$. In Table III we indicate some of the coupled states for NN scattering consistent with the generalized Pauli principle ($L+S+T=$odd).

For each eigenchannel the Stapp amplitudes are the following:

$$\alpha_L=e^{2i\delta_L}-1,\quad \alpha_{LL}=e^{2i\delta_L}-1\ , \tag{A1}$$

$$\alpha_{L,L\pm1}\equiv\alpha_{j\mp1,j}=\cos^2\epsilon_j e^{2i\delta_{j\mp1,j}} +\sin^2\epsilon_j e^{2i\delta_\pm}-1\ , \tag{A2}$$

$$=\cos^2\epsilon_j e^{2i\delta_{j\mp1,j}}-1\ , \tag{A3}$$

$$\alpha^{L-1}\equiv\alpha^j=\tfrac{1}{2}\sin2\epsilon_j(e^{2i\delta_\pm}-e^{2i\delta_\mp})\ , \tag{A4}$$

$$=i\sin2\epsilon_j e^{i(\delta_++\delta_-)}\ , \tag{A5}$$

where for coupled channels the δ's refer to the Blatt-Biedenharn convention, and the $\bar\delta$'s to Stapp's "bar" phases.

We use the Bystricky, Lechanoine, and Lehar[36] $S-K$ wave phase tabulation, smoothed to produce continuous amplitudes over the energy range 10—750 MeV. The amplitudes $M^J_{LL'}$ are first calculated in the eigenchannel α basis directly from the phases. These are then converted to the spin basis amplitudes,

$$\langle S,m_{S'}=\nu'\,|\,M\,|\,S,m_S=\nu\rangle\equiv M_{\nu'\nu},\quad S=0(\equiv s),1\ , \tag{A6}$$

via the expansions

$$M^s=2C\sum_L{}'P_L(\theta)(2L+1)M^L_L\ , \tag{A7}$$

$$M_{11}=C\sum_L{}''P_L(\theta)\left\{(L+2)M^{L+1}_{LL}+(2L+1)M^L_{LL}+(L-1)M^{L-1}_{LL}-[(L+1)(L+2)]^{1/2}M^{L+1}_{LL+2}-[(L-1)L]^{1/2}M^{L-1}_{LL-2}\right\}, \tag{A8}$$

$$M_{10}=\sqrt2C\sum_L{}''P^1_L(\theta)\left\{M^{L+1}_{LL}-M^{L-1}_{LL}+\left[\frac{L+2}{L+1}\right]^{1/2}M^{L+1}_{LL+2}-\left[\frac{L-1}{L}\right]^{1/2}M^{L-1}_{LL-2}\right\}, \tag{A9}$$

$$M_{1-1}=C\sum_L{}''P^2_L(\theta)\left\{\frac{1}{L+1}M^{L+1}_{LL}-\frac{2L+1}{L(L+1)}M^L_{LL}+\frac{1}{L}M^{L-1}_{LL} -[(L+1)(L+2)]^{-1/2}M^{L+1}_{LL+2}-[L(L-1)]^{1/2}M^{L-1}_{LL-2}\right\}, \tag{A10}$$

$$M_{01}=\sqrt2C\sum_L{}''P^1_L(\theta)\left\{-\left[\frac{L+2}{L+1}\right]M^{L+1}_{LL}+\left[\frac{2L+1}{L(L+1)}\right]M^L_{LL}+\left[\frac{L-1}{L}\right]M^{L-1}_{LL} +\left[\frac{L+2}{L+1}\right]^{1/2}M^{L+1}_{LL+2}-\left[\frac{L-1}{L}\right]^{1/2}M^{L-1}_{LL-2}\right\}, \tag{A11}$$

$$M_{00}=2C\sum{}''P_L(\theta)\left\{(L+1)M^{L+1}_{LL}+LM^{L-1}_{LL}+[(L+1)(L+2)]^{1/2}M^{L+1}_{LL+2}+[(L-1)L]^{1/2}M^{L-1}_{LL-2}\right\}, \tag{A12}$$

where

$$P^m_L(\cos\theta)=\sin^m\theta\frac{d^m}{dx^m}P_L(\cos\theta)\ , \tag{A13}$$

$$C=\begin{cases}\dfrac{1}{2ik}: & \text{for Stapp NN amplitudes}\\ \dfrac{1}{4\pi^2}: & \text{for pA } V \text{ or } T \text{ expansions}\end{cases}, \tag{A14}$$

the "$'$" indicates two times the sum over even L for NN scattering, and the "$''$" two times the sum over odd L for NN scattering. Note that for the "nonidentical" pA scattering, there is no restriction to even or odd L and no factor of 2. The Coulomb amplitude gets added to the singlet M^s and M_{11},M_{00} amplitudes.

The $A-E$ amplitudes are calculated as the linear combinations:

$$A=\tfrac{1}{2}(M_{11}+M_{00}-M_{1-1}) , \tag{A15}$$

$$B=\tfrac{1}{2}(M_{11}+M_{ss}+M_{1-1}) , \tag{A16}$$

$$C=\tfrac{1}{2}(M_{11}-M_{ss}+M_{1-1}) , \tag{A17}$$

$$D=\tfrac{1}{2}(M_{00}+M_{1-1}-M_{11})/2\cos\theta , \tag{A18}$$

$$E=i(M_{10}-M_{01})/\sqrt{2} . \tag{A19}$$

APPENDIX B: REFERENCE FRAME RELATIONS WITH SPIN

We consider the scattering of two particles in an arbitrary frame of reference

$$\vec{k}+\vec{p}\rightarrow\vec{k}'+\vec{p}' , \tag{B1}$$

where three-momentum—but not energy—is conserved:

$$\vec{k}'=\vec{k}+\vec{q},\quad \vec{p}'=\vec{p}-\vec{q} , \tag{B2}$$

$$E(k)+E(p)\neq E(k')+E(p') . \tag{B3}$$

$\vec{p}$ is given by the "optimal" choice [Eq. (2.5)],

$$\vec{p}_0=\frac{-\vec{k}}{A}+\frac{A-1}{2A}\vec{q} . \tag{B4}$$

We wish to relate these momenta in the c.m.

$$\vec{\kappa}+-\vec{\kappa}\rightarrow\vec{\kappa}'+-\vec{\kappa}' . \tag{B5}$$

The Aaron, Amado, and Young[49] (AAY) prescription is

$$\vec{\kappa}=\vec{Q}-a\vec{K} , \tag{B6}$$

where

$$a=a(\vec{k},\vec{k}')=\frac{\vec{Q}\cdot\vec{K}}{K_0[K_0+s_{in}(\vec{k},\vec{k}')]} , \tag{B7}$$

$$K=(K_0,\vec{K})=\{[E_p(k)+E_N(p)],\vec{k}+\vec{p}\} , \tag{B8}$$

$$\begin{aligned}\vec{Q}&=\tfrac{1}{2}[\vec{k}-\vec{p}-K(m_p^2-m_N^2)/s_{in}] ,\\ &=\tfrac{1}{2}(\vec{k}-\vec{p}) ,\\ &=[(3A+1)\vec{k}-(A-1)\vec{k}']/4A ,\end{aligned} \tag{B9}$$

$$\begin{aligned}s_{in}&=(k^\mu+p^\mu)^2\\ &=2m_n^2+2E_p(k)E_N(p)-2\vec{k}\cdot\vec{p} .\end{aligned} \tag{B10}$$

Similar relations hold for $\vec{\kappa}'$, e.g.,

$$a'=a(\vec{k}',\vec{k}) . \tag{B11}$$

If all substitutions are now made, we can express $\vec{\kappa}$ and $\vec{\kappa}'$ in the simple forms

$$\vec{\kappa}=b\vec{k}+c\vec{k}',\quad \vec{\kappa}'=b'\vec{k}'+c'\vec{k} , \tag{B12}$$

$$b=b(a)=\frac{3A+1}{4A}-a\frac{A-1}{2A},\quad b'=b(a') , \tag{B13}$$

$$c=c(a)=-\frac{(A-1)}{4A}-a\frac{A-1}{2A},\quad c'=c(a') . \tag{B14}$$

These relations then permit us to relate the three unit vectors in the NN and pA frames

$$\hat{n}=\frac{\vec{k}\times\vec{k}'}{|\vec{k}\times\vec{k}'|},\quad \hat{l}=\frac{\vec{k}+\vec{k}'}{|\vec{k}+\vec{k}'|},\quad \hat{m}=\frac{\vec{k}'-\vec{k}}{|\vec{k}'-\vec{k}|}=\hat{q} , \tag{B15}$$

$$\tilde{n}=\frac{\vec{\kappa}\times\vec{\kappa}'}{|\vec{\kappa}\times\vec{\kappa}'|}=\hat{n} , \tag{B16}$$

$$\tilde{m}=\frac{\vec{\kappa}'-\vec{\kappa}}{|\vec{\kappa}'-\vec{\kappa}|}=e(\theta)\hat{l}+d(\theta)\hat{m} , \tag{B17}$$

$$\tilde{l}=\frac{\vec{\kappa}+\vec{\kappa}'}{|\vec{\kappa}+\vec{\kappa}'|}=f(\theta)\hat{l}+g(\theta)\hat{m} , \tag{B18}$$

$$e(\theta)=\tfrac{1}{2}(c'-c+b'-b)\,|\vec{k}'+\vec{k}|\,/\,|\vec{\kappa}'-\vec{\kappa}| , \tag{B19}$$

$$d(\theta)=\tfrac{1}{2}(b+b'-c-c')\,|\vec{k}'-\vec{k}|\,/\,|\vec{\kappa}'-\vec{\kappa}| , \tag{B20}$$

$$f(\theta)=\tfrac{1}{2}(b+b'+c+c')\,|\vec{k}'+\vec{k}|\,/\,|\vec{\kappa}'+\vec{\kappa}| , \tag{B21}$$

$$g(\theta)=\tfrac{1}{2}(c-c'+b'-b)\,|\vec{k}'-\vec{k}|\,/\,|\vec{\kappa}'+\vec{\kappa}| , \tag{B22}$$

Further study regarding spin transformations with the full Breit-to-c.m. Wigner spin rotation can be found in the work of McNeil, Ray, and Wallace.[50]

---

*Present address: Departamento de Física, Universidad de Antioquia, Medellín, Colombia.

[1]For recent reviews, see Proceedings of the University of Alberta/TRIUMF Workshop, Studying Nuclei with Intermediate Energy Protons, Edmonton, 1983, edited by J. M. Greben, TRIUMF Report No. TRI-83-3; *The Interaction Between Medium Energy Nucleons in Nuclei—1982,* Proceedings of the Workshop on the Interaction Between Medium Energy Nucleons, AIP Conf. Proc. No. 97, edited by H. O. Meyer (AIP, New York, 1983); W. T. H. van Oers, TRIUMF Report No. TRI-77-3, 1977.

[2]A. W. Thomas and R. H. Landau, Phys. Rep. 58, 121 (1980).

[3]R. H. Landau, Phys. Rev. C 15, 2127 (1977); for kinematics, see also S. A. Gurvitz, J.-P. Dedonder, and R. D. Amado, *ibid.* 19, 149 (1979).

[4]G. W. Hoffmann, L. Ray, M. Barlett, W. R. Coker, J. McGill, G. S. Adams, G. J. Igo, F. Irom, A. T. M. Wang, C. A. Whitten, Jr., R. L. Bourdrie, J. F. Amann, C. Glasshausser, N. M. Hintz, G. S. Kyle, and G. S. Blanpied, Phys. Rev. C 24, 541 (1981), and references therein.

[5]L. G. Arnold, B. C. Clark, R. L. Mercer, and P. Schwandt, Phys. Rev. C 23, 1949 (1981); L. G. Arnold, B. C. Clark, and R. L. Mercer, *ibid.* 21, 1899 (1980).

[6]S. W.-L. Leung and H. S. Sherif, Can. J. Phys. 56, 1116 (1978); H. S. Sherif, Phys. Rev. C 19, 1649 (1979).

[7]A. Herzenberg and E. J. Squires, Nucl. Phys. 19, 280 (1960).

[8]H. S. Sherif, M. S. Abdelmonem, and R. S. Sloboda, University of Alberta report, 1983.

[9]B. Z. Kopeliovich and I. K. Potashnikova, Yad. Fiz. 13, 1032 (1971) [Sov. J. Nucl. Phys. 13, 593 (1971)].

[10]H. Lésniak, L. Lésniak, and A. Tekou, Nucl. Phys. A267, 503 (1976).

[11]N. P. Goldstein, A. Held, and D. G. Stairs, Can. J. Phys. 48, 2629 (1970).

[12]H. Langevin-Joliot, Ph. Narboni, J. P. Didelez, G. Duhamel, L. Marcus, and M. Roy-Stephen, Nucl. Phys. A158, 309 (1970).
[13]R. Frascaria *et al.,* Lett. Nuovo Cimento 2, 240 (1971).
[14]R. Beurtey *et al.,* Saclay Report as private communication of D. Hasell.
[15]R. Frascaria, I. Brissaud, N. Marty, M. Morlet, F. Reide, A. Willis, R. Beurtey, A. Boudard, M. Garcon, G. A. Moss, Y. Terrien, and W. T. H. van Oers, Phys. Lett. 66B, 329 (1977).
[16]M. Blecher, K. Gotow, E. T. Boschitz, W. R. Roberts, J. S. Vincent, P. C. Gugelot, and C. F. Perdrisat, Phys. Rev. Lett. 24, 1126 (1970).
[17]J. Fain, J. Gardes, A. Lefort, L. Meritet, J. F. Pauty, G. Peynet, M. Quertou, and F. Vazeille, Nucl. Phys. A262, 413 (1976).
[18]J. Berthot, thesis, Centre d'Orsay, Université Paris-Sud; J. Berthot, G. Douhet, J. Gardes, L. Méritet, M. Querrou, T. Têtefort, F. Vazeille, J. P. Burq, M. Chemarin, M. Chevallier, B. Ille, M. Lambert, J. P. Marin, J. P. Gerber, and C. Voltini, in *High Energy Physics and Nuclear Structure—1975* (Sante Fe and Los Alamos) Proceedings of the Sixth International Conference on High Energy Physics and Nuclear Structure, AIP Conf. Proc. No. 26, edited by R. E. Nagle and A. S. Goldhaber (AIP, New York, 1975).
[19]R. Bertini *et al.,* Saclay Report as private communication of D. Hasell.
[20]G. P. Alkhazov, S. L. Belostotsky, E. A. Damaskinsky, Yu. V. Dostsenko, O. A. Domchenkov, N. P. Kuropatkin, D. Legrand, V. N. Nikulin, O. E. Prokof'ev, M. A. Shuvaev, and S. S. Volkov, Phys. Lett. 85B, 43 (1979).
[21]T. A. Tombrello, C. Miller Jones, G. C. Phillips, and J. L. Weil, Nucl. Phys. 39, 541 (1962).
[22]D. K. Hasell, A. Bracco, H. P. Gubler, W. P. Lee, W. T. H. van Oers, R. Abegg, J. M. Cameron, L. G. Greenaius, D. A. Hutcheon, C. A. Miller, G. A. Moss, G. Roy, M. B. Epstein, D. J. Margaziotis, A. W. Stetz, and H. Postma, Bull. Am. Phys. Soc. 27, 568 (1982); (private communication).
[23]I. Reichstein, D. R. Thompson, and Y. C. Jang, Phys. Rev. 3, 2139 (1971).
[24]P. Heiss and H. H. Hackenbroich, Nucl. Phys. A182, 522 (1972).
[25]G. W. Greenlees and Y. C. Tang, Phys. Lett. 34B, 359 (1971).
[26]G. Bizard and A. Osmont, Nucl. Phys. 364, 333 (1981).
[27]Ph. Narboni, Nucl. Phys. A205, 481 (1973).
[28]A. Chaumeaux, V. Layly, and R. Schaeffer, Ann. Phys. (N.Y.) 116, 247 (1978).
[29]S. J. Wallace, in *Advances in Nuclear Physics,* edited by J. Negele and E. Vogt (Plenum, New York, 1981), Vol. 12, p. 135.
[30]S. A. Gurvitz, Y. Alexander, and A. S. Rinat, Ann. Phys. (N.Y.) 93, 152 (1975); 98, 346 (1976).
[31]Y. Alexander and R. H. Landau, Phys. Lett. 84B, 292 (1979).
[32]S. J. Wallace and Y. Alexander, Phys. Lett. 90B, 346 (1980).
[33]J. Bystricky, F. Lehar, and P. Winternitz, J. Phys. (Paris) 39, 1 (1978).
[34]R. H. Landau, S. C. Phatak, and F. Tabakin, Ann. Phys. (N.Y.) 78, 299 (1973).
[35]K. L. Schwarz, H. Zingl, and L. Mathelitsch, University of Graz Report No. UTP 02/79, 1979.
[36]J. Bystricky, C. Lechanoine, and F. Lehar, Saclay Report No. D Ph PE.79-01, 1979.
[37]S. A. Gurvitz, Phys. Rev. C 24, 29 (1981).
[38]I. V. Falomkin *et al.,* Nuovo Cimento 57A, 111 (1980); R. Mach and M. G. Sapozhnikov, Dubna Report No. E4-82-191, 1982, submitted to J. Phys. G.
[39]J. S. McCarthy, I. Sick, R. R. Whitney, and M. R. Yearian, Phys. Rev. Lett. 25, 884 (1970).
[40]R. G. Arnold, B. T. Chertok, S. Rock, W. P. Schütz, Z. M. Szalata, D. Day, J. S. McCarthy, F. Martin, B. A. Mecking, I. Sick, and G. Tamas, Phys. Rev. Lett. 40, 1429 (1978).
[41]H. Collard, R. Hofstadter, E. B. Hughes, A. Johansson, M. R. Yearian, R. B. Day, and R. T. Magner, Phys. Rev. 138, B57 (1965).
[42]J. M. McMillan, Phys. Rev. C 3, 1702 (1971).
[43]M. I. Haftel and F. Tabakin, Nucl. Phys. A158, 1 (1970).
[44]R. H. Landau, Comput. Phys. Commun. 28, 109 (1982).
[45]M. L. Godberger and K. M. Watson, *Collision Theory* (Wiley, New York, 1964).
[46]A. Picklesimer, P. Tandy, and R. Thaler, Phys. Rev. C 25, 1215 (1982).
[47]P. Tandy (private communication).
[48]H. P. Stapp, T. Y. Ypsiltantis, and N. Metropolis, Phys. Rev. 105, 302 (1957).
[49]R. Aaron, R. D. Amado, and J. E. Young, Phys. Rev. 174, 2022 (1968).
[50]J. A. McNeil, L. Ray, and S. J. Wallace, Phys. Rev. C 27, 2123 (1983).